Large-angle scattering of light ions in the weakly screened Rutherford region

H. H. Andersen, F. Besenbacher, P. Loftager, and W. Möller*
Institute of Physics, University of Aarhus, DK-8000 Aarhus C, Denmark
(Received 26 November 1979)

Total differential cross-section ratios for scattering of H^+, He^+, and Li^+ ions incident on bismuth-zinc and gold-carbon systems have been measured. The energy dependence of the cross sections was measured for each species at a fixed laboratory backscattering angle ($\varphi_{lab} = 170°$), using an amorphous carbon target implanted with 10-keV Zn^+ and Bi^+ at a depth of ~ 2.7 $\mu g/cm^2$. Angular distributions ($\varphi_{lab} = 15°$, ..., 170°) were measured for helium ions at four different energies, using selfsupporting vacuum-deposited polycrystalline carbon and gold foils. For the case of backscattering, the cross-section ratios $(d\sigma)_{Bi}/(d\sigma)_{Zn}$ deviate significantly from both the Rutherford-scattering law and the Lindhard, Nielsen, and Scharff differential-scattering cross section. The deviations of the absolute cross sections from the Rutherford cross sections amount to 3.5% for 1-MeV and 16% for 0.2-MeV helium on bismuth. The experimental results are in good agreement with exact classical differential-scattering cross sections based on the Lenz-Jensen and Dirac-Hartree-Fock-Slater atomic potentials. Simple analytical formulas describing the energy and angular dependence of the cross sections are presented.

I. INTRODUCTION

A precise knowledge of the ion-atom differential-scattering cross section is indispensable for the description and understanding of phenomena such as stopping, radiation damage, sputtering, Coulomb excitation, and channeling. The demand for precise cross sections is particularly strong for MeV light ions since such data are necessary for ion-beam analysis, where the Rutherford-backscattering (RBS) method has proved to be one of the most powerful techniques for elemental-composition analysis of materials in the near-surface region.

A simplified description of the ion-atom scattering in the near-Rutherford-scattering region, has been presented by Lindhard, Nielsen, and Scharff[1] (hereinafter referred to as LNS). These authors described ion-atom collisions in terms of similarity properties and gave a comprehensive description of the elastic-scattering cross section.

The LNS theory is based on a Thomas-Fermi similarity description of elastic atomic collisions. The two main constituents are the following: (i) The interatomic screening is given by the Thomas-Fermi (TF) or the Lenz-Jensen (LJ) screening function, which depends only on the interatomic distance measured in units of a screening length a. This implies that the scattering cross sections may be given with only the relative kinetic energy in reduced TF units and the scattering angle as variables. (ii) A small-angle perturbation calculation (momentum approximation) shows that the cross section depends on the product of the relative kinetic energy and scattering angle only. A further approximation is then introduced by a wide-angle extrapolation, which results in the energy-times-angle scaling. Thus Lindhard *et al.*[1] found that the elastic-scattering cross section is a function of a single parameter only, which is proportional to the product of the projectile energy and recoil energy in the collision. Hence, it suffices to calculate only one single universal scattering function for a given potential. This procedure leads to a significant simplification in the calculation of the cross section for elastic-collision processes but at the same time to some loss of accuracy. For very small distances of closest approach, the LNS scattering cross section approaches the exact Rutherford-scattering law. In this limit, the wide-angle extrapolation holds exactly.

In spite of the extensive use of the LNS scattering cross section for theoretical calculations, surprisingly few experimental and theoretical investigations have been made of its limit of validity. Most of the published experimental data have claimed uncertainties of 10–40%. New information on the validity of the LNS theory, however, has been obtained recently by accurate measurements with both solid[2-5] and gaseous[6,7] targets, but for small scattering angles only.

Andersen *et al.*[2,3] and Knudsen and Møller Petersen[4,5] have investigated the weakly screened Rutherford region for small scattering angles ($\varphi_{lab} \leq 15°$). Their measurements confirmed the two basic similarity scaling properties of the LNS theory, (i) the energy-times-angle scaling for fixed collision systems with atomic numbers (Z_1, Z_2) and (ii) the (Z_1, Z_2) scaling, according to which the differential elastic-scattering cross section for all combinations of Z_1 and Z_2 is given by a single reduced scattering function. Furthermore, the absolute values of the measured cross sections generally agreed well with the theoretical prediction based on the TF screening function. Loftager *et al.*[6,7]

also investigated the weakly screened region[6] but mainly that for larger distances of closest approach, corresponding to scattering in strongly screened potentials.[7] In both regions, the scaling properties inherent in the LNS theory was confirmed for small scattering angles. Their absolute experimental cross sections for scattering of hydrogen and helium by neon in the weakly screened region[6] agreed well with the theoretical results based on the TF universal potential. For the extensive study of single-scattering cross sections with a xenon target in the strongly screened region,[7] the absolute experimental results lie between the theoretical results based on the TF and LJ potentials, respectively. A new universal potential, yielding 10–30% higher cross sections than the LJ potential is suggested[7] by these experimental findings.

However, no systematic experimental investigation of the error associated with the wide-angle extrapolation in the LNS theory has been performed in the weakly screened Rutherford region. In this region, where the distance of minimum approach is of the order of the K-shell radius of the target atom, different interatomic potentials nearly coincide so that the experiments primarily check the wide-angle extrapolation of the cross sections. In addition, in this region, precise cross-section data are needed in order to establish corrections to the Rutherford cross section for H^+, He^+, and Li^+ ions at energies typical for a RBS analysis experiment.

II. EXPERIMENTAL

In order to achieve a high degree of accuracy, relative cross sections were measured. Thus we avoid two of the major problems in absolute measurements, namely the determination of the absolute solid angle of the detector and the ion current. An excellent discussion of the major experimental problems involved in obtaining absolute scattering yields with a high precision has been presented by the Chalk River group.[8]

The experimental setup is shown schematically in Fig. 1. The ion beam obtained from a 2-MV Van de Graaf accelerator was collimated by two variable apertures, both set at 1×1 mm.^{2} These were placed 3 m apart, which results in a beam divergence of less than 0.04°. The incoming beams were H^+, $^4He^+$, and $^7Li^+$. Sufficiently intense (~5nA), well-collimated Li^+ ion beams were obtained from the Van de Graaf accelerator by placing a piece of lithium metal in the rf ion source, which operated with argon as support gas.

The targets were mounted in a two-axis goniometer placed in a 30-cm diameter scattering chamber. An oil diffusion pump and a liquid-nitrogen cooling trap, which surrounded the goniometer, provided a vacuum better than 1×10^{-6} torr during the experiment. No carbon build-up on the target was detectable. The particles backscattered from the target were registered and energy analyzed by means of a cooled surface-barrier detector (sensitive area 25 mm^2, energy resolution ~12 keV for 2-MeV He^+). The pulses from the detector were processed by standard electronics and, via an ADC, fed into a NORD-12 satellite computer programmed for running in a PHA mode. The beam current was always low enough ($\leq$100 nA) to keep pile-up effects at a negligible level. The target surface and detector positions were oriented in the scattering plane with respect to the incident beam to a precision of ±0.1° by means of a laser beam prealigned to be collinear with the particle beam. The sensitive area of the 170° detector was limited by a 1-mm wide slit prependicular to the scattering plane.

To investigate the energy dependence of the

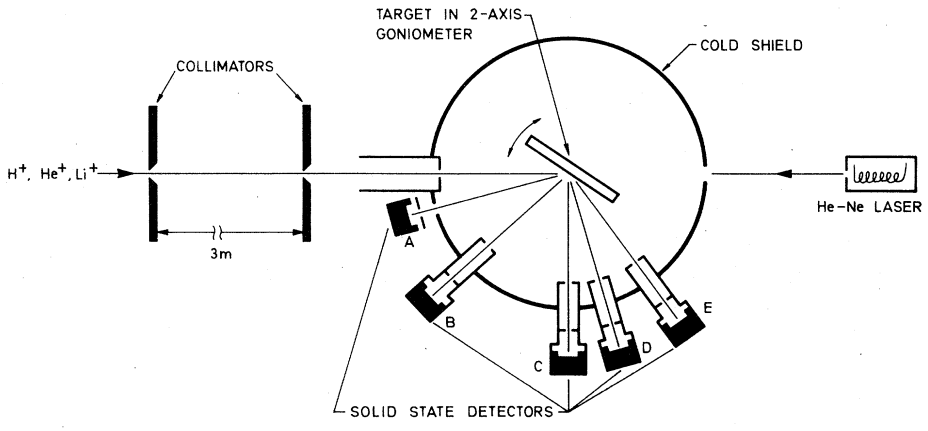

FIG. 1. Experimental setup employed for scattering angles $170° \geq \varphi_{lab} \geq 58°$.

weakly screened Rutherford cross section for wide-angle scattering, we measured the ratios $(d\sigma)_{Bi}/(d\sigma)_{Zn}$ of differential-scattering cross sections for (1.0–1.6)-MeV $^1H^+$, 0.3–2.3 MeV $^4He^+$, and (0.2–1.6)-MeV $^7Li^+$ ions on bismuth and zinc as functions of primary energy with detector A (Fig. 1) at a scattering angle of 170°. As backing material for the targets, commercially available amorphous carbon wafers were used, which were Syton polished to achieve optically flat surfaces. Into these targets, 3.1×10^{15} Bi^+/cm^2 and 2.5×10^{16} Zn^+/cm^2 were implanted at an energy of 10 keV. During implantation, the ion beam was swept continuously over a target area of 1 cm^2 to obtain a homogeneous implantation, and the carbon wafer was heated to ~100 °C to avoid contamination build-up at the target. The implantation energies were chosen so that Bi^+ and Zn^+ would penetrate to approximately the same projected depth. Using the tabulation of Winterbon,[9] we obtain the results for the mean range R_m and the range straggling for Zn^+ and Bi^+ in carbon given in Table I.

It is seen that the ranges agree to within 6%, while the range straggling for bismuth is smaller by a factor of 1.85 than that for zinc. Since these numbers are at variance with those given by L'Ecuyer *et al.*,[8] we measured the most probable ranges, using the high-resolution RBS[10,11] obtained by tilting the target 67.5° off normal and employing 1-MeV He^+ ions backscattered through 170°. These experimental, most probable ranges R_p^{expt} are also given in Table I, and it is seen (i) that the most probable depths for zinc and bismuth agree to within 8%, which is also the accuracy of the data, and (ii) that the measured ranges for bismuth and zinc are systematically higher than those obtained from the Winterbon tabulations.[9] These facts are in agreement with recent range studies of energetic, heavy ions in silicon and aluminum.[12] Possible consequences of the small difference of the most probable depths are discussed in Sec. IV A.

To investigate the angular dependence of the cross section for a fixed energy, the experimental setup was equipped with further four surface-barrier detectors placed at scattering angles of 143.9°, 92.6°, 78.4°, and 57.7° with the target tilted 60° off normal. In order to suppress slit-edge scattered particles, another 2-mm-diameter collimator was inserted into the beam line. Furthermore, in front of each detector was placed a special collimator tube with a 2-mm and a 1.5-mm diameter collimator inserted. For these measurements, the targets consisted of evaporated 20-$\mu g/cm^2$ polycrystalline carbon films, onto which 20-Å gold was evaporated. The self-supporting part had a diameter of 6 mm.

Since it was not possible to separate the carbon and gold peaks at lower angles, we have used a setup nearly identical to that previously described by Andersen *et al.*[13] for measurements down to ~15°. In this target chamber the pressure was less than 1×10^{-6} torr, which was obtained by a diffusion pump in conjunction with a liquid nitrogen cooling trap. Another trap prevented hydrocarbon from the accelerator from entering the chamber. The incoming beam was collimated by variable apertures, each set to $\frac{1}{2}\times\frac{1}{2}$ mm^2, placed 1.5 m apart. The targets, a 20-$\mu g/cm^2$ evaporated carbon foil and a 400-Å evaporated gold foil, both of them polycrystalline, were mounted at fixed positions along the circumference of the target wheel (for details, see Ref. 13). A step-motor was used to rotate the wheel, thereby changing the irradiated target. Two fixed, limited by 1 mm slits, detectors were inserted at scattering angles of 135° and 45°, respectively, and a third one with a 1-mm diameter collimator was movable in two mutually perpendicular directions in a plane perpendicular to the beam. This latter detector was used for measurements at scattering angles of 24.5°, 19.5°, and 14.5°. In this experiment as well as in the one discussed above, only relative cross sections were measured, and the precise knowledge of the scattering angles used is of no consequence for the precision of our results. The carbon and gold targets were irradiated alternately for two seconds each under simultaneous routing of the PHA memory, which permits the allotment of a different memory fraction to each target. The measuring cycle was repeated more than 50 times in each run so that the fluctuation in the beam current was sufficiently averaged in order to obtain the ratio of the scattering yields from carbon and gold.

III. THEORY

In their similarity theory of classical atomic scattering, Lindhard, Nielsen, and Scharff[1] (LNS) showed that the interaction between two atoms

TABLE I. Results for the theoretical mean range and range straggling and for the experimental most probable range for Zn and Bi in carbon.

	R_m ($\mu g/cm^2$)	$\langle\Delta R^2\rangle^{1/2}$ ($\mu g/cm^2$)	R_p^{expt} ($\mu g/cm^2$)
10-keV Bi→C	1.73	0.301	2.59
10-keV Zn→C	1.84	0.558	2.79

can be approximated by the universal interatomic potential:

$$V^{\mathrm{LNS}}(r)=(Z_1Z_2e^2/r)\varphi(r/a)\,. \tag{1}$$

Here, the screening function φ, such as e.g., the atomic TF or LJ screening function, is a function only of the internuclear distance r in units of the screening radius:

$$a=0.8853a_0(Z_1^{2/3}+Z_2^{2/3})^{-1/2}\,. \tag{2}$$

In Eqs. (1) and (2), Z_1 and Z_2 are the atomic numbers of ion and target atom, respectively, e is the electron charge, and a_0 is the Bohr radius. The potential in Eq. (1) implies similarity of all ion-atom potentials.

In the calculation of the elastic differential cross section, LNS used the momentum approximation applicable for classical small-angle scattering, which leads to a cross section depending only on the product of the center-of-mass scattering angle θ and the reduced, dimensionless TF energy ϵ, where

$$\epsilon=\frac{a}{Z_1Z_2e^2}E_{\mathrm{c.m.}}=E_{\mathrm{lab}}\frac{aM_2}{Z_1Z_2e^2(M_1+M_2)}\,. \tag{3}$$

Here $E_{\mathrm{c.m.}}$ and E_{lab} are the center-of-mass and the laboratory kinetic energies, and M_1 and M_2 are the masses of projectile and target atom, respectively. Finally, LNS introduced a wide-angle extrapolation by substituting

$$\theta\epsilon \to 2\epsilon\sin\frac{\theta}{2}\equiv 2t^{1/2}\,. \tag{4}$$

The approximate universal differential-scattering cross section may then be written as

$$d\sigma=-\pi a^2(dt/2t^{3/2})f(t^{1/2})\,. \tag{5}$$

The reduced scattering function $f(t^{1/2})$ is calculated numerically for a universal potential given by Eq. (1), as shown in Ref. 1. It should be noted that in case of Rutherford scattering, where $f_R(t^{1/2})=\frac{1}{2}t^{-1/2}$, Eq. (5) holds exactly.

The exact classical calculation of the scattering cross section involves the integral

$$\theta=\pi-2p\int_{r_0}^{\infty}\frac{dr}{r^2h(r)},\qquad h(r)=[1-p^2/r^2-V(r)/E_{\mathrm{c.m.}}]^{1/2}\,, \tag{6}$$

where p is the impact parameter and r_0 is the distance of closest approach given by $h(r_0)=0$.

Once θ is known as a function of p, the differential scattering cross section is obtained from the formula

$$\left(\frac{d\sigma}{d\Omega}\right)_{\mathrm{c.m.}}=-\frac{p}{\sin\theta}\frac{dp}{d\theta}\,. \tag{7}$$

Standard numerical procedures have been used for the calculation of Eqs. (6) and (7) (Ref. 6). The problem associated with the singularity in the denominator in the integrand of Eq. (6) is solved as shown in Ref. 15 by substituting $r=r_0/(1-u^2)$.

According to Eqs. (4) and (5), the f value corresponding to the center-of-mass cross section is obtained from

$$f(t^{1/2})=\frac{8\epsilon}{a^2}\sin^3\frac{\theta}{2}\left(\frac{d\sigma}{d\Omega}\right)_{\mathrm{c.m.}}\,. \tag{8}$$

Contrary to the universal scattering function f_{LNS} of the LNS similarity theory, which depends only on $t^{1/2}$, exact values of $(d\sigma/d\Omega)_{\mathrm{c.m.}}$ give f_{exact} as a function of two parameters, ϵ and $t^{1/2}$. This is illustrated in Fig. 2 (from Ref. 6), which shows f_{exact} divided by f_{LNS} given by Eq. (5) as a function of ϵ and $t^{1/2}$ for the TF and LJ potentials. As expected, the deviation from the universal f_{LNS} function is in general largest for backward scattering ($t^{1/2}=\epsilon$). We note that with ϵ decreasing from large values, the deviation of f_{exact} from f_{LNS} increases from 0 to -20% at $\epsilon=1$, returns to 0 at $\epsilon\sim 1\times10^{-2}$, and then becomes positive and increasing. This is in qualitative agreement with the estimate of Lindhard *et al.*,[1] based on power potentials and with the exact results for the Bohr potential obtained by Everhart *et al.*[16] From Fig. 2 it is further seen that in the weakly screened Rutherford region, the corrections to f_{LNS} depend only slightly on the specific potential, while this is not the case in the strongly screened region.

The TF and LJ potentials are derived from the statistical theory of the atom[14] and are therefore unable to account for shell effects. In our case, where $Z_1\ll Z_2$, an improved description may be based on a potential resulting from Dirac-Hartree-Fock-Slater (DHFS) relativistic electron densities.[17] The atomic potential of the target atom may be used to represent the interatomic potential to a first approximation, yielding $(Z_1Z_2e^2/r)\varphi(r)$ with $\varphi=\varphi_{\mathrm{DHFS}}$, the case of atomic screening. An improved interatomic potential is given by $(Z_1Z_2e^2/r)\varphi(ra_a/a)$, where $a/a_a=Z_2^{1/3}/(Z_1^{2/3}+Z_2^{2/3})^{1/2}$ is the ratio of the screening length of Eq. (2) and a_a that is obtained from Eq. (2) for $Z_1=0$. This latter case of "universal" screening was shown by LNS to be a good approximation in the Thomas-Fermi case in Eq. (1).

Since exact classical calculations have to be carried out for each individual system, it is desirable for practical uses to have a simple analytical formula for the correction to the Rutherford cross section. Such a formula may be found by a procedure analogous to that used by Lindhard[18] to calculate the Barkas correction to the Bethe stopping formula.

In a typical RBS experiment (for example, 2-

MeV helium ions backscattered through 170° from a given target), the major part of the deflection occurs at distances smaller than the K-shell radius of the target atom. The reason that the screening nevertheless influences the scattering is that, due to the presence of the electron cloud, the projectile experiences less repulsion from the target nucleus during its penetration of the electron cloud

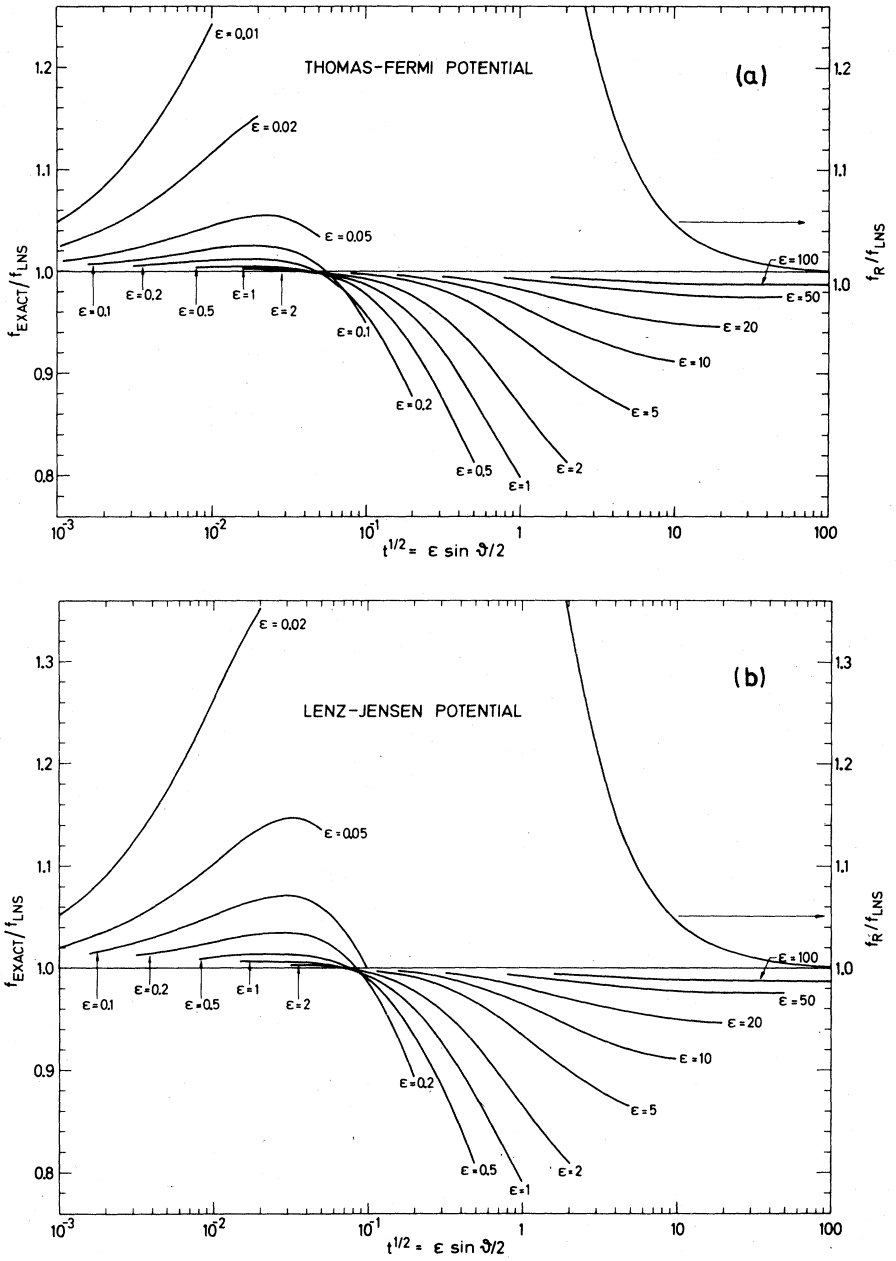

FIG. 2. Theoretical cross-section ratios with the reduced energy of Eq. (3) as a parameter for (a) the Thomas-Fermi and (b) the Lenz-Jensen interatomic potentials [see Eq. (1)]. It is observed that exact total differential-scattering cross sections represented by f_{exact} [see Eq. (8)] in the near Rutherford-scattering region ($t^{1/2} \gtrsim 10$) for backward scattering deviate up to 9% from the corresponding similarity cross sections f_{LNS} given by Lindhard, Nielsen, and Scharff (Ref. 1) and from the Rutherford cross section f_R. We may add that although the LJ and TF predictions coincide in the near Rutherford-scattering region, they differ by a factor of 2 at $t^{1/2} = 0.01$ and still more at smaller $t^{1/2}$ values. The experimental results of the present investigation have ϵ values ranging from 5 to 1300 and $t^{1/2}$ values from 2 to 1300.

and therefore less deceleration than in the unscreened Rutherford case. We may thus assume Rutherford scattering with an effective kinetic energy increased by an amount V_1, where $-V_1$ is the potential energy of the projectile at the center of the electron cloud due to the electrons alone, but with conservation of angular momentum. The effective relative kinetic energy is therefore given by

$$\tfrac{1}{2}mv^{*2}=\tfrac{1}{2}mv^2+V_1=E_{\mathrm{c.m.}}+V_1\,, \tag{9}$$

where m is the reduced mass for the projectile-target system. With the above assumptions, the correction to the Rutherford cross section for backscattering angles is easily derived since the differential-scattering cross section for Rutherford scattering is given by $(d\sigma/d\Omega)_R=(dp/d\theta)^2$. If p denotes the initial impact parameter and p^* the effective one due to the larger effective velocity v^*, and θ and θ^* are the corresponding scattering angles, we have

$$\left(\frac{d\sigma}{d\Omega}\right)^A\equiv\left(\frac{dp}{d\theta^*}\right)^2=\left(\frac{v^*}{v}\right)^2\left(\frac{dp^*}{d\theta^*}\right)^2=\left(\frac{v}{v^*}\right)^2\left(\frac{dp}{d\theta}\right)^2=\left(\frac{v}{v^*}\right)^2\left(\frac{d\sigma}{d\Omega}\right)_R. \tag{10}$$

The first part of this equation expresses conservation of angular momentum, while the subsequent substitution of $dp/d\theta$ for $dp^*/d\theta^*$ utilizes the fact that $dp/d\theta=-b/4$ for $\theta=180^\circ$ and analogously for $dp^*d\theta^*$ with the collision diameter $b=2Z_1Z_2e^2/mv^2$. In an abbreviated notion, the simple correction formula for backscattering angles is

$$\frac{d\sigma^A}{d\sigma_R}=\frac{v^2}{v^{*2}}=\frac{1}{1+V_1/E_{\mathrm{c.m.}}}\,. \tag{11}$$

The general expression for the interatomic potential given by Eq. (1) allows an estimation of the additional kinetic energy V_1 as follows:

$$V(r)\simeq\frac{Z_1Z_2e^2}{r}\left(1+\varphi'(0)\frac{r}{a}\right)=\frac{Z_1Z_2e^2}{r}+\varphi'(0)\left(\frac{e^2}{a_0}\right)\frac{Z_1Z_1(Z_1^{2/3}+Z_2^{2/3})^{1/2}}{0.8853}\,, \tag{12}$$

that is (in eV)

$$V_1=-30.72\varphi'(0)Z_1Z_2(Z_1^{2/3}+Z_2^{2/3})^{1/2}\,. \tag{13}$$

Since $\varphi'_{LJ}(0)=-1.586$, we find (in eV)

$$V_1^{LJ}=48.73\ Z_1Z_2(Z_1^{2/3}+Z_2^{2/3})^{1/2}\,. \tag{14}$$

The approximation that leads to Eq. (11) may also be used to predict the angular dependence of the correction. The result is not satisfactory, however, and will not be reproduced here. To properly incorporate the angular dependence of the deviation from the Rutherford cross section, it is necessary to carry out an exact classical calculation of the cross section for a reasonable potential.

An approximate potential, which in a simple way reflects the outer screening discussed above, is given by Eq. (12) in connection with a cutoff:

$$U(r)=\begin{cases}Z_1Z_2e^2/r-V_1\,, & \text{for } r<r_c=-a/\varphi'(0)\\ 0\,, & \text{for } r>r_c\,.\end{cases} \tag{15}$$

With this potential inserted into Eq. (6), the cross section can be calculated analytically with the following result:

$$\frac{d\sigma^B}{d\sigma_R}=\frac{(1+\frac{1}{2}V_1/E_{\mathrm{c.m.}})^2}{\{1+V_1/E_{\mathrm{c.m.}}+[\frac{1}{2}(V_1/E_{\mathrm{c.m.}})(1/\sin\frac{1}{2}\theta)]^2\}^2}\,. \tag{16}$$

If cubic and higher-order terms in $(V_1/E_{\mathrm{c.m.}})$ are neglected, a series expansion gives

$$\frac{d\sigma^C}{d\sigma_R}=1-\frac{V_1}{E_{\mathrm{c.m.}}}+\left(\frac{V_1}{E_{\mathrm{c.m.}}}\right)^2(\tfrac{5}{4}-\tfrac{1}{2}\sin^2\tfrac{1}{2}\theta)\,. \tag{17}$$

From this formula it is seen that the angular dependence of $d\sigma/d\sigma_R$ is weak over a rather broad angular region.

Wenzel and Whaling,[19] van Wijngaarden,[20] and recently L'Ecuyer *et al.*[8] have carried out an analytical calculation similar to that given above. With the specific purpose to obtain a correction to the Rutherford formula for RBS-analysis experiments, Wenzel and Whaling[19] and L'Ecuyer *et al.*[8] arrived at the following first-order, angular-independent formula for the screening correction:

$$\frac{d\sigma^D}{d\sigma_R}=1-\frac{V_1}{E_{\mathrm{c.m.}}}\,. \tag{18}$$

Wenzel and Whaling[19] used Foldy's[21] semiempirical estimate for $V_1(V_1^F=32.6\ Z_1Z_2^{7/5}$ eV), while the Chalk River group[8] used $V_1^*=48.73\ Z_1Z_2^{4/3}$ eV, corresponding to atomic screening in Eq. (12).

IV. RESULTS AND DISCUSSIONS

A. Energy dependence at a fixed, large scattering angle

In Fig. 3 is shown a typical energy spectrum with detector A (Fig. 1) placed at $\varphi_{1\mathrm{ab}}=170^\circ$. For a given energy, the ratio between the scattering yield from bismuth and zinc is given by

$$\frac{Y_{\mathrm{Bi}}}{Y_{\mathrm{Zn}}}=\frac{n_{\mathrm{Bi}}}{n_{\mathrm{Zn}}}\frac{g(\theta)_{\mathrm{Bi}}}{g(\theta)_{\mathrm{Zn}}}\frac{(d\sigma/d\sigma_R)_{\mathrm{Bi}}}{(d\sigma/d\sigma_R)_{\mathrm{Zn}}}\frac{(d\sigma_R)_{\mathrm{Bi}}}{(d\sigma_R)_{\mathrm{Zn}}}\,. \tag{19}$$

Here n denotes the target density and $g(\theta)$ is the factor converting from center-of-mass to laboratory quantities given by

$$g(\theta)=\frac{(\gamma+\cos\theta)^2\sin\theta}{(1+\gamma\cos\theta)\sin\varphi_{1\mathrm{ab}}\cos^2\varphi_{\mathrm{lab}}}\,,\quad \gamma=\frac{M_1}{M_2}\,. \tag{20}$$

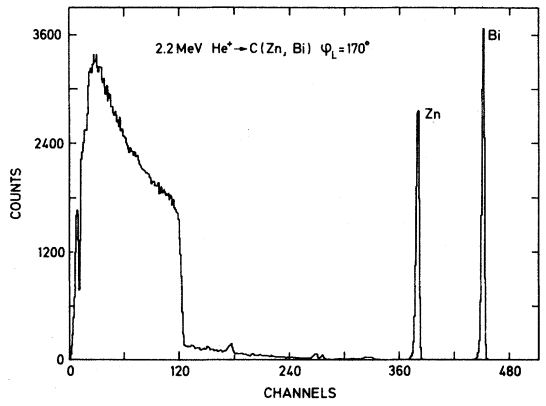

FIG. 3. Backscattering spectrum from the Bi-Zn two-component target. The target was prepared by implanting $3.1\times10^{15}/\text{cm}^2$ Bi^+ and $2.5\times10^{16}/\text{cm}^2$ Zn^+ into amorphous C, each at 10 keV. Slight contaminations of O, Al, Si, and Ar do not influence the results within the quoted accuracy.

The ratio of the measured cross sections relative to the Rutherford cross section may then be determined from the ratio of the scattering yields if the ratio between the target-area densities of bismuth and zinc is known. The high-energy H^+ data were normalized to the theoretical predictions to determine the ratio n_{Bi}/n_{Zn}, which could not be measured with sufficient accuracy during the implantation. We believe that such a normalization procedure is justified because for protons in the energy region $1 \lesssim E_H \lesssim 1.6$ MeV, the $t^{1/2}$ values are so large ($t^{1/2}=327$ for zinc and $t^{1/2}=87$ for bismuth for 1-MeV hydrogen scattered through 170°), and hence the r_0 values so small, that the theoretical cross-section ratios are nearly independent of the potential assumed and consequently have a high degree of confidence. The cross-section ratio was calculated numerically for the DHFS potential with universal screening. Inserting this ratio into Eq. (19), we determine $(n_{Bi}/n_{Zn})_{expt}$ by averaging over the result for the different energies. For all H^+ spectra, the zinc and bismuth peaks were separated, but some influence of pile-up effects from the enhanced $^{12}C(p,p')^{12}C$ nuclear scattering was seen. After a background subtraction of the order of 1%, the n_{Bi}/n_{Zn} ratio was determined with an accuracy of 1.5%. With this ratio inserted in Eq. (19), the ratio between the measured cross sections relative to the Rutherford cross section for He^+ and Li^+ bombardment was determined. The cross-section ratios are plotted in Fig. 4 for the H^+, He^+, and Li^+ projectiles as a function of energy. It was possible clearly to separate the zinc and the bismuth peaks in all cases. Since there were no continuous background and contamination problems, the uncertainty on the cross-section ratios is only 1.5%, which mainly stems from counting statistics.

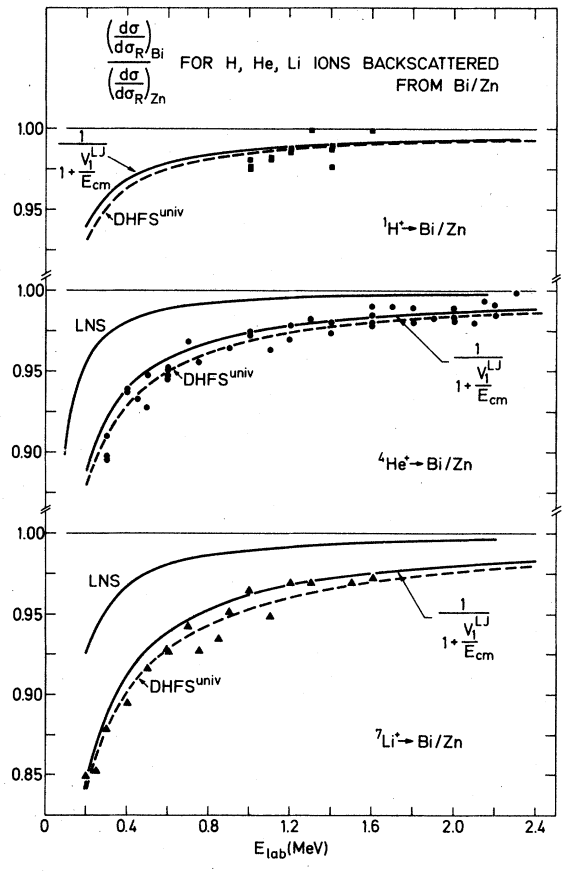

FIG. 4. Differential-scattering cross-section ratios relative to the Rutherford cross section as a function of the incident (lab) energy at the deflection angle $\varphi_{lab}=170°$. Experimental results are compared with predictions from exact classical calculations for the DHFS potential with universal screening, with the LNS similarity results for the LJ potential, and with the simple analytical expression given by Eqs. (11) and (14).

From Fig. 4 it is seen that the cross-section ratio $(d\sigma/d\sigma_R)_{Bi}/(d\sigma/d\sigma_R)_{Zn}$ decreases for decreasing energy and, further, deviates from both the Rutherford and the LNS similarity predictions, in agreement with the results in Fig. 2. In Fig. 4, the experimental results are compared with the analytical formula (11) with V_1 given by V_1^{LJ} [Eq. (14)] and with exact classical results for the DHFS potential with universal screening. Both of the theoretical curves are in good agreement with the experimental results, but within the stated accuracy, we may conclude that the curve $DHFS^{univ}$ is superior.

Besides the screening effects mentioned above that were caused by atomic electrons, there are several other effects causing corrections to the

Rutherford trajectory that might influence the results in Fig. 4. These effects[22] may be treated in the same way as the screening correction in Eq. (11), i. e., in terms of an additional kinetic energy V_1. We note the following points. (i) The vacuum polarization leads to the following increase in energy,

$$V_1^{VP}/E_{c.m.} = 1.55 \times 10^{-3} \ln[96.86/r_0(\theta)] \sin(\theta/2), \tag{21}$$

where r_0 (in fm) is the distance of closest approach. It is seen that the correction to the Rutherford formula shows only a slight dependence on energy and projectile mass. In all cases, the correction to the cross-section ratio is less than 0.25%. (ii) The relativistic correction is given by

$$\frac{V^{rel}}{E_{c.m.}} = \frac{E_{c.m.}}{m_0 c^2} \frac{\sin^2(\theta/2)}{1+\sin(\theta/2)}, \tag{22}$$

and it is easily seen to have no influence on the cross-section ratio. (iii) The dipole polarization effect and the effect due to nuclear forces are both negligible for the present energies and ion-atom systems. Finally, the slight difference in implantation depth of zinc and bismuth (Table I) gives rise to a small energy correction. For both helium and lithium ions, the correction to the cross-section ratio is in all cases less than 0.3%. All data shown in Fig. 4 have been corrected for this effect.

An estimate of the kinematical influence of the inelastic energy loss in single collisions (roughly assessed to be 2% of the kinetic energy) shows that it affects the cross-section ratio at most by 0.2%; this correction is neglected. Furthermore, the condition for applying classical scattering theory[1] in the cases treated here is clearly fulfilled.

In order to evaluate the different theoretical calculations of and the analytical approximation to the weakly screened Rutherford cross section, in Fig. 5 we consider for the specific case of the He → Bi system the results of these predictions relative to the cross section for the DHFS potential with universal screening as a function of energy. The cross section $d\sigma$ (DHFS^{univ}) is chosen as a reference since it is believed to be the most accurate one, a fact that is corroborated by the experimental findings in Fig. 4. From Fig. 5 the following is seen. (i) For high energies, the cross sections agree to within 0.2% while increased splitting occurs for decreasing energies. (ii) Introduction of universal rather than atomic screening lowers the cross sections by approximately 1% and 0.1% at $\epsilon \sim 4$ and $\epsilon \sim 85$, respectively. (iii) The difference between the LJ and the DHFS cross sections is ~2% for $\epsilon \sim 4$ and decreases with increasing energy. (iv) The cross section $d\sigma^A$ given by Eqs. (11) and (14) has a maximum deviation of 0.8% from $d\sigma$ (DHFS^{univ}) for the energies in question. This is compared to the energy dependence of the cross section $d\sigma^D$ [Eq. (18)] used by L'Ecuyer *et al.*[8] which, for energies down to $\epsilon \sim 13$, agrees to within 0.5% with $d\sigma$(DHFS^{univ}), while the deviation becomes excessive for lower ϵ values. The latter circumstance is due to the fact that $d\sigma^D$ only represents a first-order expansion, while inclusion of the second-order term leads to a cross section $d\sigma^C$ [Eq. (17)], which deviates very little from $d\sigma^A$. The use of V_1^{LJ} [Eq. (14)] in $d\sigma^A$ instead of the expression for atomic screening $V_1^* = 49 \text{ eV } Z_1 Z_2^{4/3}$ used by L'Ecuyer *et al.*[8] improves the agreement with $d\sigma$ (DHFS^{univ}) by an amount comparable to the difference between the atomic and universal screening curve in Fig. 5.

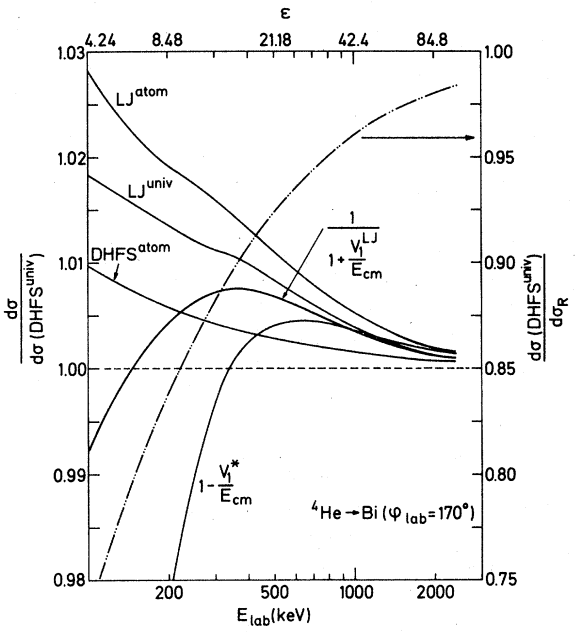

FIG. 5. Different theoretical predictions for the screening correction factor to the Rutherford cross section for backscattering of ^{4}He from Bi. Dot and dash line (right-hand scale): Exact cross sections for the DHFS potential with universal screening. Solid lines (left-hand scale): Exact results for different potentials (with atomic and universal screening) and simple analytical predictions, Eqs. (11) and (18) with V_1 given by V_1^{LJ} and V_1^*, respectively, all relative to the DHFS^{univ} results.

In Fig. 5 is further shown the ratio between the DHFS^{univ} cross section and the Rutherford cross section. A comparison of this curve with the curve DHFS^{univ} for the helium case in Fig. 4, shows that the deviation of the latter curve and thus also of the experimental cross-section ratios from the

Rutherford predictions is caused mainly by the characteristics of the He→Bi cross section. The reason is that for a given energy, the $t^{1/2}$ value with zinc as the target is nearly a factor of 4 larger than that with a bismuth target, leading to much smaller deviations from the Rutherford and the LNS similarity cross sections for zinc than for bismuth, according to Fig. 2. The same is true for hydrogen and lithium projectiles. Note in particular that non-negligible deviations from the Rutherford cross section occur for energies regularly used in analytical work.

B. Angular dependence of the cross section for fixed energy

Above we have investigated the energy dependence of the deviations from the Rutherford and the LNS scattering formulas for backscattering. However, it is also important to study the angular dependence of these deviations, as illustrated in Fig. 2.

For a given beam energy and scattering angle, the ratio between the scattering yields from gold and carbon is given by an equation similar to Eq. (19). The ratio between the gold and carbon area densities is determined by normalizing the data for the scattering of 1.5-MeV He^+ through the largest scattering angles to the $DHFS^{univ}$ results. For measurements at scattering angles smaller than 45°, it has been necessary to correct the gold cross sections for the influence of multiple scattering[3,23] since the measurements do not directly yield $d\sigma(\theta)$ but rather a thickness-dependent reduced scattering yield. The largest correction amounts to 21.8%, which is applied to 300-keV helium scattered through 14.5°, corresponding to the lowest value of $t^{1/2}=1.74$. For higher $t^{1/2}$ values, the correction decreases rapidly, and it is negligible in the carbon case.

In Fig. 6 is plotted the ratio between gold and carbon cross sections relative to the Rutherford cross section as a function of φ_{lab}. Since the variation of the deviations of the cross sections from the Rutherford predictions is attributed mainly to the gold results, and since the cross-section ratios in Fig. 6 for $\varphi_{lab} > 90°$ are close to the Rutherford predictions, the angle-independent screening correction [Eq. (11)] gives a good description of the deviation from the Rutherford formula for almost all RBS-analysis experiments ($E_{He} \gtrsim 300$ keV, $\varphi_{lab} \gtrsim 90°$). The experimental results in Fig. 6 are compared with the predictions from exact classical calculations based on the DHFS potential with universal screening, with the LNS similarity results for the LJ potential, and with the results from the angle-dependent analytical formula [Eq. (16)] with V_1 given by V_1^{LJ} [Eq. (14)]. It is seen

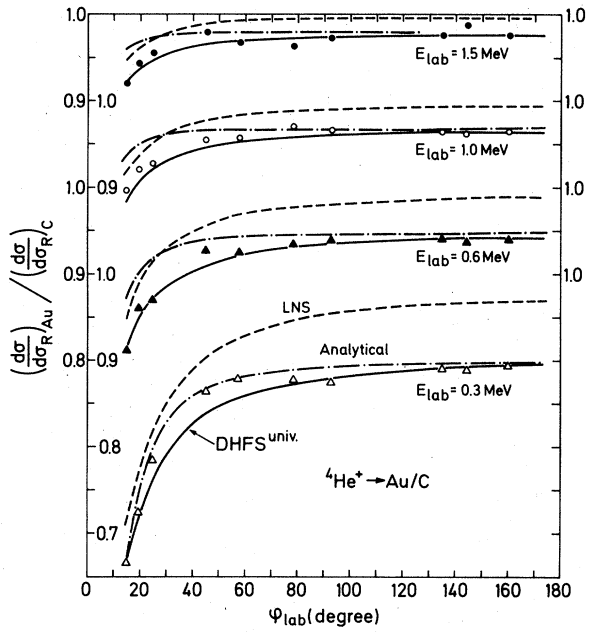

FIG. 6. Angular dependence of the differential-scattering cross-section ratios (relative to the Rutherford prediction) for the Au-C system. The experimental results are compared with those from an exact classical calculation based on DHFS radial densities, with the LNS similarity results for the Lenz-Jensen potential, and with the results from the analytical formula [Eq. (16)].

that the deviations from the LNS prediction decrease with decreasing φ_{lab}, in agreement with expectations from Fig. 2. Both the analytical and the $d\sigma$ ($DHFS^{univ}$) results are in good agreement with the experimental data, but once again, the $DHFS^{univ}$ curve is superior.

C. Validity of analytical correction formulas

The above results show that the energy dependence of the experimental cross-section ratios for backscattering within 1% may be represented by the analytical expression in Eq. (11) in the entire energy region studied and that the angular dependence for a fixed energy ($E_{lab} \geq 300$ keV) for $\varphi_{lab} \geq 45°$ also within 1% is represented by Eq. (16), in both cases with V_1 given by V_1^{LJ} [Eq. (14)]. The latter equation may, in fact, also be used to represent all of the backscattering results within 1%.

At this place, a few comments on the basis for the success of the analytical formula would be appropriate. For that purpose, Fig. 7 shows the interaction energy for the He-Bi system in terms of the screening function $\varphi = \varphi_{LJ}$ for the Lenz-Jensen potential as a function of the internuclear separation r in units of the screening length ($x = r/a$) as well as three more curves of relevance to our discussion. One of these is a curve denoted $\varphi - x\varphi'$

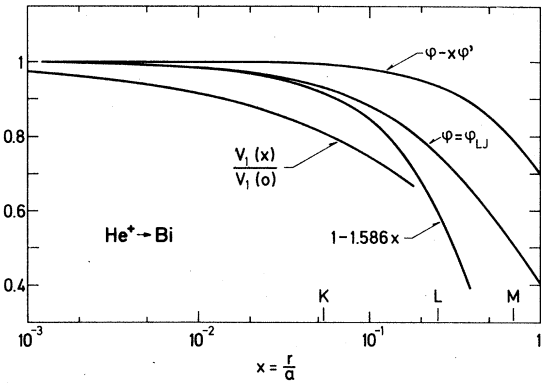

FIG. 7. The figure allows comparison of the interatomic LJ screening function φ_{LJ} (see text) to the approximation $1-1.586x$ of Eqs. (15) and (14) that leads to the correction formula of Eq. (16). $V_1(x)$ denotes the gained kinetic energy (or the negative of the potential energy) due to the attraction of the projectile by the electron distribution. $V_1(0)$ appears in the correction formula for backward scattering [see Eqs. (11) and (13)]. Finally, $\varphi - x\varphi'$ represents the interatomic force corresponding to $\varphi = \varphi_{LJ}$. The force deviates only little from the pure Coulomb force for $x < 0.1a$. The letters K, L, and M indicate magnitudes of the radii of the corresponding electron shells of the Bi atom.

representing the force $(Z_1Z_2e^2/r^2)(\varphi - x\varphi')$, another curve is denoted $V_1(x)/V_1(0)$, where $V_1(x)$ is the gained kinetic energy at a distance x caused by the electron distribution, and finally the curve denoted $1-1.586x$, representing the approximate potential $(Z_1Z_2e^2/r)[1+\varphi'(0)x]$ of Eqs. (12) and (19) used for the derivation of the correction formula (16). In Fig. 7 we have furthermore indicated the radii of the K, L, and M shells of bismuth.

We first consider the ratio $1/[1+V_1(0)/E_{c.m.}]$ of Eq. (11) for backscattering. The derivation of this expression presupposed pure Rutherford scattering with the additional kinetic energy $V_1(0)$, and one might intuitively expect Eq. (11) to hold only when the main deflection occurs well inside the K shell of the target atom. However, this is not so since Eq. (11) turns out to hold even for backscattering with smallest separation larger than two times the K-shell radius (for 200-keV Li-Bi). To understand this finding, we observe (Fig. 7) that the force, contrary to φ, even at such relatively large separations, deviates only little from the unscreened Coulomb force, and the fact that $V_1(x)$ is 20–30% smaller than $V_1(x)$ in this range further counteracts the effect of the diminished force.

To complete the discussion of Eq. (11), it should be said that the above argument is only part of the truth since the differential cross section for scattering with closest distances of approach near the K-shell radius, but with smaller deflection angles, deviates substantially from predictions of the angular dependence based on the assumptions that lead to Eq. (11).

The angular dependence of the cross-section ratios is adequately given by Eq. (16) for collisions with closest distances of approach r_0 smaller than approximately two times the K-shell radius of the heavier target atom. Figure 7 shows that the screening function $1-1.586x$ that leads to Eq. (16) actually represents φ_{LJ} quite closely in this range. Furthermore, we may note that the approximate potential yields a repulsive force equal to that for the unscreened case for $r < r_c = 0.63a$. The success of Eq. (16) for collisions with $r_0/a < 0.1$ is thus a result of a force that is zero for $r > 0.63a$ and equal to $Z_1Z_2e^2/r^2$ for $r < 0.63a$.

V. COMPARISON WITH OTHER MEASUREMENTS

There are very few experimental investigations of the deviation from the Rutherford and the LNS cross sections for wide-angle scattering in the weakly screened Rutherford region, the main reason being that a high degree of accuracy is needed.

The Chalk River group[8] has given an excellent discussion of all the experimental problems involved in measuring absolute RBS scattering yields. A major part of their experimental program was to measure the screening correction as a function of Z_1, Z_2, and E_{lab}. In an experiment similar to the present one, they measured the relative scattering cross sections $d\sigma(\mathrm{Bi})/d\sigma(\mathrm{Mn})$ at a fixed, large scattering angle for ^{4}He, ^{12}C, ^{14}N, ^{16}O, and ^{20}Ne ions at energies $0.1 \leq E_0\,(\mathrm{MeV})/Z_1 \leq 2$. Based on the first-order correction given by Eq. (18), they express the screening correction as a function of the variable E_{lab}/Z_1. Applying our procedure (see above) to their data, we obtain an n_{Mn}/n_{Bi} ratio, which is 1% lower than theirs. Their results then show the same tendency as ours, namely that the experimental cross-section ratios are lower than the prediction from Eq. (18) for energies down to 100 keV/amu.

Van Wijngaarden *et al.*[24,25] measured differential-scattering cross sections for 9–75-keV H, He, B, and N ions scattered on a thermal beam of mercury atoms in the range of $2.8^\circ \leq \varphi_{lab} \leq 60^\circ$, i. e., for $10^{-2} \lesssim t^{1/2} \lesssim 1$. Since their data are vitiated by experimental uncertainties up to ±15%, it is difficult to draw specific conclusions, but the tendency is that at small scattering angles, the experimental data are in good agreement with LNS predictions for the TF potential, but at large scattering angles, they follow the exact TF predictions.

Van Wijngaarden *et al.*[20] also measured the differential-scattering cross sections for scattering to an angle of 136.4° of (50–110)-keV ^{1}H, ^{4}He, ^{7}Li,

and ^{11}B from a gold target. From Fig. 8 in Andersen *et al.*,[2] it is seen that within the experimental accuracy, the data of Ref. 20 agree both with the LNS predictions for the TF potential and with the data of Andersen *et al.*[2] This is in contradiction to the present measurements and also to the theoretical results in Fig. 2 that deviate 10–20% from the LNS predictions for the relevant $(t^{1/2},\epsilon)$ values, $1.5 \lesssim t^{1/2} \lesssim 10$, $1 \lesssim \epsilon \lesssim 10$.

ACKNOWLEDGMENTS

We are much indebted to J. U. Andersen and E. Laegsgaard for the help and guidance received through numerous discussions, to J. Bøttiger for taking part in the early measurements and to A. Grandjean for her assistance in the preparation of the manuscript.

*Permanent address: Institut für Experimentalphysik I, Ruhr-Universität Bochum, D-4630 Bochum, Federal Republic of Germany.

[1]J. Lindhard, V. Nielsen, and M. Scharff, Kgl. Danske Videnskab. Selskab, Mat. Fys. Medd. 36, No. 10 (1968).
[2]H. H. Andersen, J. Bøttiger, and H. Knudsen, Phys. Rev. A 7, 154 (1973).
[3]H. H. Andersen and H. Knudsen, Phys. Rev. A 10, 733 (1974).
[4]H. Knudsen and P. Møller Petersen, Radiat. Eff. 28, 147 (1976).
[5]H. Knudsen and P. Møller Petersen, J. Phys. B. 11, 455 (1978).
[6]P. Loftager and J. E. Andersen (unpublished).
[7]P. Loftager, F. Besenbacher, O. S. Jensen, and V. S. Sørensen, Phys. Rev. A 20, 1443 (1979).
[8]J. L'Ecuyer, J. A. Davies, and N. Matsunami, Nucl. Instrum. Methods 160, 337 (1979).
[9]K. B. Winterbon, *Ion Implantation Range and Energy Deposition Distribution*, edited by D. K. Brice (Plenum, New York, 1975), Vol. 2.
[10]J. S. Williams, Nucl. Instrum. Methods 149, 207 (1977).
[11]J. S. Williams and W. Möller, Nucl. Instrum. Methods 157, 213 (1978).
[12]J. L. Combasson, B. W. Farmery, D. McCulloch, G. W. Neilson, and M. W. Thompson, Radiat. Eff. 36, 149 (1978).
[13]H. H. Andersen, H. Knudsen, and V. Martini, Nucl. Instrum. Methods 149, 137 (1978); H. H. Andersen and J. Bøttiger, Phys. Rev. B 4, 2105 (1971).
[14]P. Gombas, *Handbuch der Physik*, edited by S. Flügge (Springer, Berlin, 1956), Vol. 36, p. 109.
[15]M. T. Robinson, Report No. ORNL-3493, 1963 (unpublished).
[16]E. Everhart, G. Stone, and R. J. Carbone, Phys. Rev. 99, 1287 (1955).
[17]D. A. Liberman, D. T. Cromer, and J. T. Waber, Comput. Phys. Commun. 2, 107 (1971).
[18]J. Lindhard, Nucl. Instrum. Methods 132, 1 (1976).
[19]W. A. Wenzel and W. Whaling, Phys. Rev. 87, 499 (1952).
[20]A. van Wijngaarden, E. J. Brimner, and W. E. Baylis, Can. J. Phys. 48, 1835 (1970).
[21]L. L. Foldy, Phys. Rev. 83, 397 (1951).
[22]K. Alder and A. Winther, *Electromagnetic Excitation* (North-Holland, Amsterdam, 1975).
[23]P. Sigmund and K. B. Winterbon, Nucl. Instrum. Methods 119, 541 (1974).
[24]A. van Wijngaarden, B. Miremadi, and W. E. Baylis, Can. J. Phys. 50, 1938 (1972).
[25]A. van Wijngaarden and W. E. Baylis, Phys. Rev. A 7, 937 (1973).